crystals

MDPI

Article

The Polymorphism of 2-Benzoyl-*N,N*-diethylbenzamide

Lygia S. de Moraes [1,*], Jie Liu [1], Elumalai Gopi [1], Ryusei Oketani [1], Alan R. Kennedy [2] and Yves H. Geerts [1,3,*]

[1] Laboratoire de Chimie des Polymères, Faculté des Sciences, Université Libre de Bruxelles (ULB), Boulevard du Triomphe, CP 206/01, 1050 Bruxelles, Belgium; jie.liu@ulb.be (J.L.); gopi.elumalai@ulb.be (E.G.); oketani@chem.es.osaka-u.ac.jp (R.O.)
[2] WestCHEM, Department of Pure & Applied Chemistry, University of Strathclyde, Glasgow G1 1XL, UK; a.r.kennedy@strath.ac.uk
[3] International Solvay Institutes of Physics and Chemistry, ULB—Campus Plaine—CP 231 Boulevard du Triomphe, 1050 Brussels, Belgium
* Correspondence: lygia_moraes@hotmail.com (L.S.d.M.); yves.geerts@ulb.be (Y.H.G.)

Abstract: The crystal structures of two new polymorphs of 2-benzoyl-*N,N*-diethylbenzamide were obtained after recrystallization trials with different solvents. The new forms II and III were monoclinic and crystallized in the same space group with similar *a*, *b* and *c* lengths but different β angles. The forms had no conformation differences within themselves; however, the long-range packing (>two unit cells) was not isostructural. In comparison with the previously published crystal structure, form I, different conformations and packing arrangements were observed. The new form II was thermally characterized and stable at room temperature, when heated up to its melting point and when cooled to −170 °C. Additionally, once form II was re-heated, a fourth form is observed after a phase transition from the monoclinic to the orthorhombic crystal systems, form IV.

Keywords: polymorphism; variable temperature; organic

Citation: de Moraes, L.S.; Liu, J.; Gopi, E.; Oketani, R.; Kennedy, A.R.; Geerts, Y.H. The Polymorphism of 2-Benzoyl-*N,N*-diethylbenzamide. *Crystals* **2021**, *11*, 1004. https://doi.org/10.3390/cryst11081004

Academic Editor: Josep Lluís Tamarit

Received: 11 August 2021
Accepted: 15 August 2021
Published: 22 August 2021

1. Introduction

Polymorphism occurs when identical compounds are organized in more than one repeating pattern of the solid form. A new form of a compound can occur either by varying the molecular conformation or by changes in the molecular packing in a new unit cell. Both imply changes in intermolecular interactions, such as π–π interactions, van der Waals forces and hydrogen bonds. As changing the crystalline form of the solid results in a new unit cell with different interactions between the atoms, the physical and chemical properties of each polymorph will be different from each other [1–5].

In pharmaceutical research, it is important to understand the polymorphism of compounds under non-ambient conditions of temperature and pressure to avoid changes in the crystalline structure during manufacturing, as the formation of a new polymorph can improve or minimize the effect of the drug in the human body. More importantly, analyzing a drug candidate in temperature ranges that can be reached in the manufacturing site can be an important tool to check the stability of the drug for pharmaceutical companies [6,7]. The occurrence of new forms of molecular compounds with temperature variations is a common phenomenon and has been previously reported in the literature where the phase of the new form was either obtained by single-crystal or powder X-ray diffraction [8–12].

The compound studied in this work, 2-Benzoyl-*N,N*-diethylbenzamide (BDB, Scheme 1), was first reported by Projotiva et al. (1950) as a potential candidate for antispasmodic drugs [13]. The compound was synthesized and thermally characterized, where the obtained melting point was 51.1 °C. A year later, thermal characterization of BDB was performed by Linn et al. (1951) prior to reactions between a series of *N,N*-diethylbenzamides and sodium, where the author found a higher melting point for the compound (MP = 76–77 °C), showing a possible new form of BDB [14]. In 2004, BDB was crystallized as a precursor for asymmetric synthesis by Sakamoto et al. (2004), and its

crystal structure was obtained [15]. The compound crystallized with the chiral space group $P2_12_12_1$ from a mixture of hexane and chloroform, and crystallographic data were collected at room temperature. However, the melting point of this form was not recorded. More recently, BDB has been used as a precursor for different synthesis routes of ortho-acylation of benzamides with rhodium or palladium catalyzers [16–19]. However, the relationship between form and melting point was not established for this compound.

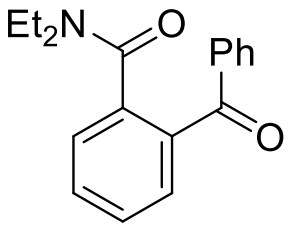

Scheme 1. Molecular structure of 2-benzoyl-*N*,*N*-diethylbenzamide (BDB).

In order to study the polymorphism of 2-benzoyl-*N*,*N*-diethylbenzamide in ambient and non-ambient temperature conditions, this work presents crystallization and thermal characterization of the BDB. Then, the compound was also analyzed by means of single-crystal and powder X-ray diffraction with variable temperatures. Finally, an assessment of the interactions in the crystal structures is also reported.

2. Materials and Methods

2.1. Synthesis, Solvent Screening and Recrystallization

Synthesis was performed using the route described by Wei et al. (2015), and details of the synthesis, as well as ^{1}H and ^{13}C NMR spectra of BDB are available in the Supporting Information (Scheme S1, Figures S1 and S2) [20].

To find a suitable solvent for the recrystallization of BDB, solubility tests with different solvents were conducted at room temperature. The solvents chosen for the screening were: acetone, ethanol, diethylether, dichloromethane, heptane and a 1:1 volume mixture of hexane and chloroform. A spatula tip of the powder was added to a 2.0 mL HPLC vial, and 0.5 mL of the solvent was added. When completely dissolved, the vial was closed, and the lid was pierced with a needle. The vial was left in the fume cupboard for slow evaporation of the solvent. All experiments were performed at room temperature.

Recrystallization was performed using the same procedure of the solvent screening with only dichloromethane or hexane:chloroform as solvents and on a larger scale.

2.2. Thermogravimetric Analysis (TGA)

TGA of BDB was measured using a Pyris 6 TGA (Perkin Elmer, Waltham, MA, USA) with dry N_2 as a purge gas. A total of 7.7890 mg of 2-benzoyl-*N*,*N*-diethylbenzamide was weighed in a ceramic crucible and heated from 30 to 500 °C with steps of 10 °C/min. The data were analyzed using TA Universal Analysis 2000 software (version 4.5A, TA Instruments, New Castle, DE, USA). Details of the experiment and degradation temperature can be observed in Table S1 and Figure S3 (SI).

2.3. Differential Scanning Calorimetry (DSC)

DSC was measured using a DSC 214 Polyma (Netzsch, Selb, Germany) with dry N_2 as a purge gas. A total of 4.224 mg of form II of BDB (powder) was sealed in an aluminum crucible with a pierced lid and heated from −50 to 90 °C with a speed of 0.50 °C/min. The crucible was cooled down to −50 °C, at a speed of 0.75 °C/min. The second heating run occurred on the same crucible, temperature range, a speed of 0.75 °C/min and a cooling speed of 1.00 °C/min. The DSC graphs were analyzed with Proteus Analysis software by Perkin Elmer, and details of melting point and melting enthalpy can be observed in Table S1 and Figure S4 (SI).

2.4. Single-Crystal X-ray Diffraction (SXD)

The crystal structure of form II was obtained at the National Crystallography Service using an XtaLAB AFC12 (Rigaku Corporation, Tokyo, Japan) diffractometer at 150 K with Mo *Kα* (λ = 0.7107 Å) radiation [21]. The crystal structure of form III was obtained using a Gemini Oxford Diffraction diffractometer at 123 K and Cu *Kα* (λ = 1.5418 Å) radiation. All data were processed with the software CrysAlis Pro version 1.171.40.82a (Rigaku Corporation, Tokyo, Japan) [22]. The structure of form II was solved using *SHELXS* [23], while the structure of form III was solved using Superflip [24]. All structures were refined using SHELXL-2018/3 [25], and all programs mentioned above were implemented within the WinGX suite [26]. The atoms, except hydrogen, had atomic coordinates and anisotropic thermal parameters refined to convergence using full-matrix least-square methods on F^2. Most H atoms bound to C were placed in geometric positions and refined with riding modes. Where possible, H atoms that were bound to O or N were found by difference syntheses and refined with isotropic displacement parameters. Where this refinement was not possible, they were added in geometrically sensible positions and refined in riding modes. Brief details of symmetry and unit cells are given in Table 1, with full crystallographic data available in the crystallographic information files. In this work, the crystal structure of 2-benzoyl-*N*,*N*-diethylbenzamide published by Sakamoto et al. (2004), is represented as form I [15]. This form crystallizes in the chiral space group $P2_12_12_1$ with lattice parameters: a = 10.937(5), b = 13.987(5), c = 9.896(4) Å and $\alpha = \beta = \gamma = 90°$. All novel crystal structures were checked with Mogul Geometry Check within the Mercury software [27,28]. The supplementary crystallographic data for this paper for forms II and III data can be obtained free of charge from CCDC.

Table 1. Crystallographic information for both forms of 2-benzoyl-*N*,*N*-diethylbenzamide.

Crystal Data		
Label/REFCODE	Form II/BERDOS01	Form III/BERDOS02
Chemical Formula	$C_{18}H_{19}NO_2$	
MW (g/mol)	281.34	
a, *b*, *c* (Å)	13.6350(6), 8.4424(3), 26.5721(9)	13.629(3), 8.4793(6), 26.626(10)
β (°)/V (Å^3)	90.966(3), 3058.3	103.25(4), 2995.2
Space Group	*I* 2/a	
Z, Z′	8/1	
T (K)	150	123
R_{int}, R_{w2}, *S*	0.0578, 0.1369, 1.026	0.0735, 0.1974, 1.075
Recrystallization solvent	hexane: chloroform	dichloromethane

2.5. X-ray Powder Diffraction (XRPD)

X-ray powder diffraction was used to confirm the bulk phase of BDB after synthesis and recrystallization. The powder was finely ground with a mortar and pestle and was mounted in the diffractometer over a glass slide. Diffraction patterns were collected with a Rigaku Ultima IV diffractometer using Cu *Kα* (λ = 1.54184 Å) radiation, with a 2*θ* range between 5 and 30°, a speed of 5°/min and steps of 0.04°. The data were refined using the Rietveld refinement tool [29,30] on *EXPO2014* software [31], and the crystal structure of form II as the input. Powder diffraction patterns were calculated from the crystal structure using the software Mercury 4.3.1 (CCDC, Cambridge, UK) [32,33].

2.6. Variable Temperature X-ray Powder Diffraction (VT-XRPD)

Powder x-ray diffraction patterns in different temperature points were obtained for BDB. Prior to the experiments, the bulk powder was analyzed with powder diffraction to confirm the phase of the product synthesized (see SI, Figure S5 for details), confirming the starting material was form II.

In the first experiment, the form II was finely ground with a mortar and pestle and mounted in the diffractometer over a glass slide, and data were collected with a Rigaku Ultima IV diffractometer using Cu *Kα* (λ = 1.54184 Å) radiation, with a 2θ range between 2 and 40°, speed of 5°/min and steps of 0.04°. Data were refined using the Rietveld refinement tool [29,30] on EXPO2014 software [31], and the crystal structure of form II as the input.

In the second experiment, powder diffraction patterns were collected using a Panalytical Empyrean X-ray diffractometer, Cu *Kα* (λ = 1.54184 Å) radiation, with a TTK 600 variable temperature stage attached. Form II was ground using a mortar and pestle and mounted on the sample holder over a zero-background film. The program on the diffractometer was set to obtain the patterns using a gonio scan with a 2θ range from 5 to 40°, a scan speed of 0.11°/s and steps of 0.13°, for 24 temperature points in the temperature range between 103 and 328 K in a vacuum environment. The unit cell parameters at variable temperatures were indexed using the EXPO2014 software [31]. Unit cell parameters and crystal structure obtained from single-crystal X-ray diffraction were used as the input. The calculated powder patterns were refined against the experimental pattern using Rietveld refinement [29,30], with a full 2θ range, automatic refinement of the profile, non-structural parameters with the Le Bail fitting [34] and line shifts.

2.7. Hirshfeld Surfaces Calculations (HS)

Hirshfeld surfaces, voids and fingerprint plots were obtained using CrystalExplorer17 software for all forms of BDB [35–38]. The crystallographic information files were used as an input, and Hirshfeld Surfaces were calculated using the Generate Surface tool with high (standard) resolution and mapped with a dnorm range between −0.1 and 1.5 Å. Voids were calculated with medium resolution and an isovalue of 0.002 e·au^{-3} and standard void cluster (unit cell + 5 Å).

3. Results and Discussion

3.1. Synthesis and Recrystallization

2-benzoyl-*N*,*N*-diethylbenzamide was synthesized in 77% yield following the procedure described in the Supporting Information, Scheme S1. ^{1}H and ^{13}C NMR spectra of BDB were obtained, and details are available in Figures S1 and S2.

The screening of suitable solvents for recrystallization was performed on a small scale. The compound was dissolved at room temperature in most of the solvents attempted: acetone, ethanol, diethylether, dichloromethane, and in a 1:1 mixture in volume of hexane and chloroform, which form an azeotrope. Once the solution was left for recrystallization, when the solvent completely evaporated, BDB formed an oil for tests with acetone, ethanol and diethylether, indicating that this form is too soluble in these solvents. However, crystals were obtained using dichloromethane and hexane:chloroform, so a larger batch of BDB was recrystallized with these solvents.

There is no evidence that the formation of a preferential form of BDB can result from the recrystallization method used, as this compound was crystallized using different routes when the melting point of the compound was also reported [13,14,19]. Sakamoto and co-workers reported the form I was prepared from a 1:1 mixture of hexane and chloroform, a solvent mixture also suitable to recrystallize form II [15]. Although the form reported by Linn and co-workers with a melting point between 76 and 77 °C was prepared from diluted ethanol solution [14], this solvent system did not provide any crystals under our attempts.

3.2. Phase Identification and Crystal Structures

The crystalline powder from the initial batch, without recrystallization, was analyzed using X-ray powder diffraction and compared with the calculated powder pattern of the previously published form of the compound, here labeled as form I [15], where a new phase of the compound was observed. The diffraction peaks were indexed, and the unit cell parameters obtained at room temperature were a = 13.732(3), b = 8.4344(16), c = 26.941(3) Å, β = 90.302(17)°, and space group $I2/a$ (R_p = 4.1%, R_{wp} = 5.3%). This new form is identified as form II. All experimental and calculated powder diffraction patterns can be observed in Figure S3 (SI).

The power diffractograms of the batch recrystallized with a mixture of hexane and chloroform showed the crystallization of the pure form II of BDB. However, form II and another form of BDB were obtained together in the same vial when the compound was recrystallized with dichloromethane. The second new form of BDB is identified as form III. It is important to note that it was not possible to isolate form I in any of these recrystallization trials. Although form III was obtained in the first recrystallization trial, other recrystallization attempts using dichloromethane only crystallized form II.

The crystal structure of two new polymorphs of BDB was obtained using single-crystal X-ray diffraction. Both forms crystallized as a racemate in the centrosymmetric space group I2/a. Crystallographic data for form II was collected at 123 K with unit cell parameters a = 13.6350(6), b = 8.4424(3), c = 26.5721(9) Å and β = 90.966(3)°, consistent with XRPD results. The crystal structure of the second polymorph, form III, was obtained at 150 K and crystallized in the same space group as form II ($I2/a$). Form III had similar lattice parameters as form II, however with an increase of the β angle: a = 13.629(3), b = 8.4793(6), c = 26.626(10) Å and β = 103.25(4)°. No unusual bond lengths and angles were found for the novel molecules. The contents of the asymmetric unit for forms I–III are illustrated in Figure 1, and details of the crystal structure can be obtained in the available crystallographic information files.

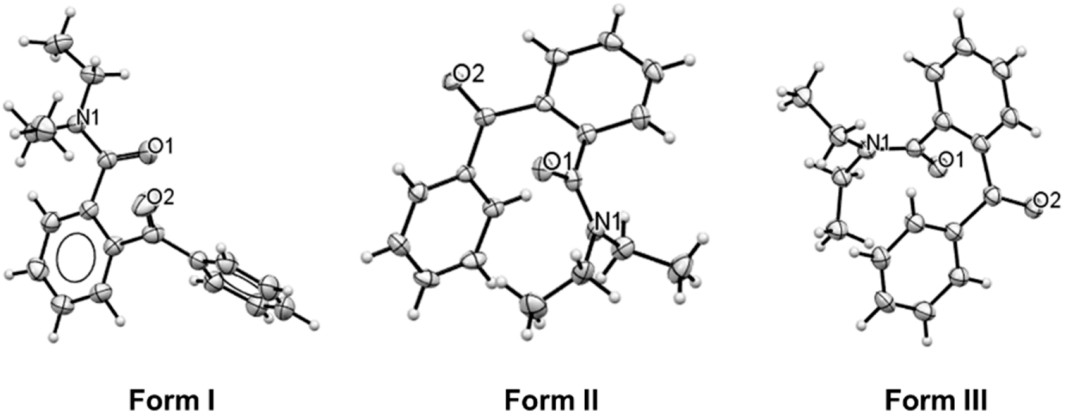

Figure 1. Contents of the asymmetric unit of forms I–III of BDB.

3.3. Database Survey

In the Cambridge Structural Database (CSD), there are seven crystal structures of compounds that maintain the same 2-benzoylbenzamide molecule as the core molecule, only by changing the composition of the groups bonded to the nitrogen atom [15,39–41]. Here, these molecules will be mentioned by their CSD reference code as follow: anti-N-Benzyl-N-ethyl-2-benzoylbenzamide (BERDUY)[15], *N*,*N*-Dibenyl-2-benzoylbenzamide (BERDAY) [15], N-Morpholino-2-benzoylbenzamide (NOSYEZ) [40], *N*,*N*-Dimethyl-2-benzoylbenzamide (OBEXOI/OBEXOI01)] [35,39], N-Methyl-N-phenyl-2-benzoylbenzamide (OBEXUO) [39] and 2′-2-(benzenecarbonyl)benzene-1-carbonylspiroindene-2,1′-isoindole-1,3,3′(2′H)-trione (SONFUZ) [41]. Molecular structures and torsion angles are given in SI, Figure S4 and

Table S1. As OBEXOI and OBEXOI01 are isostructural and have the same molecular arrangements for the core molecule, only OBEXOI will be mentioned in this section.

Conformation similarities for all compounds were obtained using the molecule overlay tool on Mercury software [32,33]. Three compounds have a similar arrangement of the core molecule when compared with the form I of BDB, with variations lower than 20% (Figure 2a): BERDUY (RMS = 10.9%), OBEXOI (RMS = 17.6%) and NOSYEZ (RMS = 14.1%). For both forms II and III of BDB, no structural similarity was observed with any of the forms in the literature.

There are seven pairs of torsion angles that describe the core molecule 2-benzoylbenzamide. For comparison, the representation for the anticlockwise rotation was described in modulus. The label for each pair is observed in Table 2, and the distribution of torsion angle values can be observed by the boxplots in Figure 2b (details in Table S1). Most torsion angle values are within an average difference between the minimum and maximum values of 27 (3)°, except the pair of torsion angles 5 where this range is smaller, and the difference between values is 7.9 (6)°. All torsion angles of BDB lies on the range described by the boxplots. For pairs 1 to 4, the outlier values belong to the racemic compounds NOSYEZ and SONFUZ, while for pairs 5 to 7, the outliers belong again to SONFUZ and to the conglomerate BERDUY.

Table 2. Details of the linear relationship between pairs of torsion angles for the core molecule, including the slope and intercept of a linear equation and the coefficient of determination for linear regression (R^2).

Pair		Atom Label	Slope	Intercept (°)	R^2
1	a	C13-C4-C10-O2	−0.95 (7)	176 (2)	0.9617
	b	C6-C4-C10-O2			
2	a	C13-C4-C10-C3	−0.92 (5)	171 (8)	0.9741
	b	C6-C4-C10-C3			
3	a	C4-C10-C3-C5	−1.18 (6)	192 (3)	0.9777
	b	C4-C10-C3-C2			
4	a	O2-C10-C3-C5	−1.16 (8)	198 (12)	0.9595
	b	O2-C10-C3-C2			
5	a	C10-C3-C2-C7	−0.04 (48)	17 (85)	0.0011
	b	C10-C3-C2-C1			
6	a	C3-C2-C1-O1	−0.89 (9)	166 (6)	0.9223
	b	O1-C1-C2-C7			
7	a	C3-C2-C1-N1	−0.82 (8)	165 (10)	0.9286
	b	N1-C1-C2-C7			

Considering the three forms of BDB and the six compounds reported in CSD with the same 2-benzoylbenzamide core molecule, there is a linear correlation between components a and b of each pair of torsion angles for the pairs 1–4, 6 and 7 (Table 2). No relationship was found between pair 5 (Figure 2c). The discrepancy is observed in the particular torsion 5b (C10-C3-C2-C1), where the values are separated into two ranges: 5b < 9°, where most racemates are found, with the exception of BERDUY (space group: $P2_12_12_1$) and 5b > 12°, where most racemic conglomerates are found, apart from NOSYEZ (space group: $P2_1/c$).

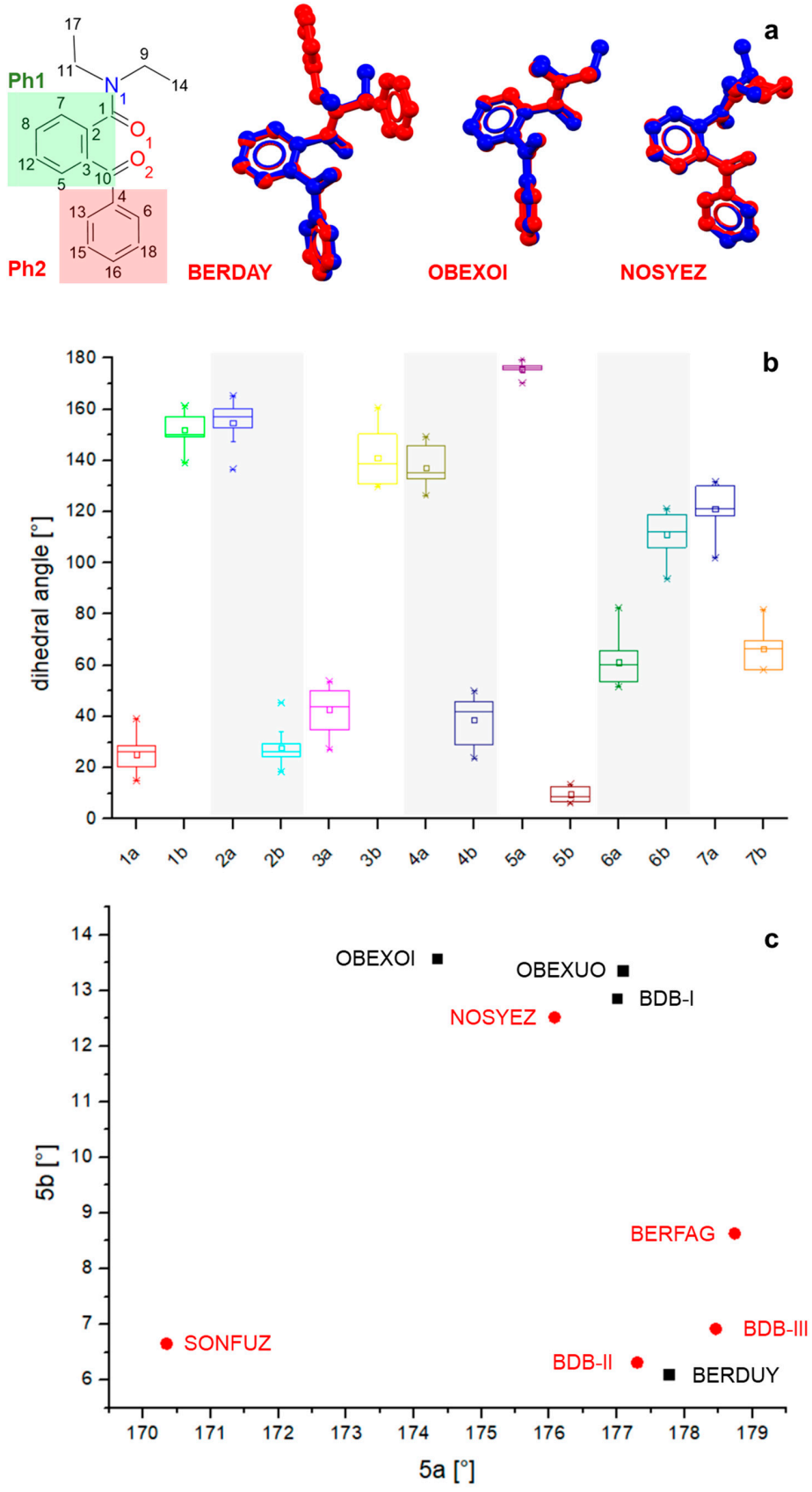

Figure 2. Structure overlay between BERDAY, OBEXOI and NOSYEZ, in red, using BDB form I as a reference in blue (**a**), boxplots for distribution of torsion angles pairs 1–7 (**b**) and scatterplot between torsion angles 5a and 5b, where compounds that crystallize as racemates are in red and compounds that crystallize as racemic conglomerates are in black (**c**).

3.4. Crystal Structure Description

2-benzoyl-*N*,*N*-diethylbenzamide has eight possible rotatable bonds that will influence the molecular arrangement within the crystal structures. As mentioned in the previous section, most of the dihedral angles that describe the differences in the three forms of BDB have a similar magnitude in modulus. For these three forms, the standard deviation for the average values is lower than 3.0%, although the rotation of atoms around a bond is opposite when comparing form I with forms II and III. The influence of the rotation direction on the molecular arrangement is illustrated for forms I and II in Figure 3a and for forms II and III in Figure 3b. The overlay of these molecules, when fixing the aromatic carbons in the phenyl group Ph1 for both forms compared, shows the inversion of the rotation direction in the torsion angles pairs 3 and 7 for form I. Consequently, the angle between the phenyl (Ph2) and diethylamide groups decrease by half between forms I and forms II and II, where the angles between C1-N1-C9 and C4-C6-C18 decrease from 82.2° for form I to 41.9° and 40.1° for forms II and III, respectively (Figure 3c,d). For details of atom numeration and torsion angles, see Table 1 and Table S1 and Figure 2a.

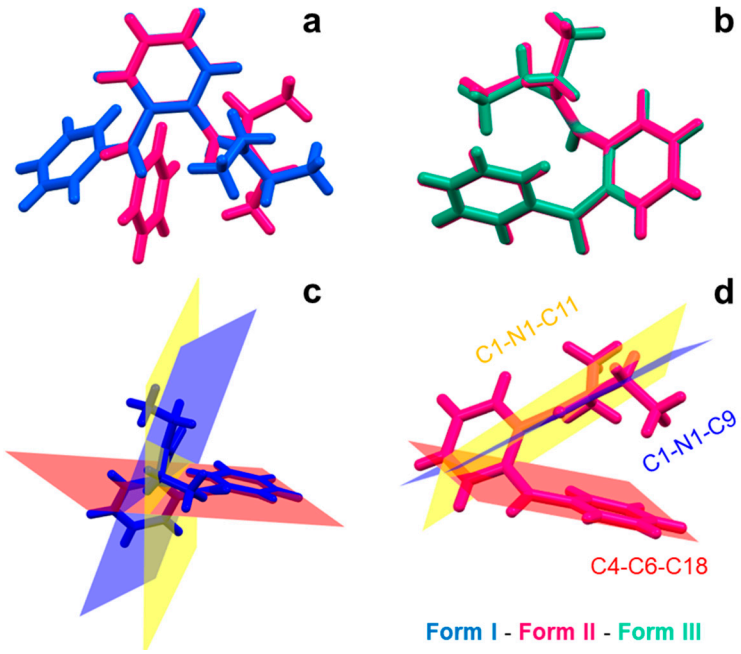

Figure 3. Molecule overlay between forms I and II (**a**), forms II and III (**b**) and the decrease of the angle between Ph1 and diethylamide groups for form I (**c**) in comparison with form II (**d**).

To better understand the intermolecular interactions occurring in all three forms of BDB, the Hirshfeld Surfaces (HS) and fingerprint plots were calculated [35–38]. Form I have a prolate shape, while forms II and III have a similar spherical shape (Figure 4a). This shape change is also a consequence of the inversion in the rotation of the torsion angles mentioned previously. Herringbone stacking is present in form I (Figure 4b) and in forms II and III (Figure 4c), however, a cofacial π–π interaction is only present in forms II and III (Figure 4d). Form II is the structure with the highest volume of voids when compared with forms I and III, which are, respectively, 59.2% and 15.3% more compact than form II (Table S2).

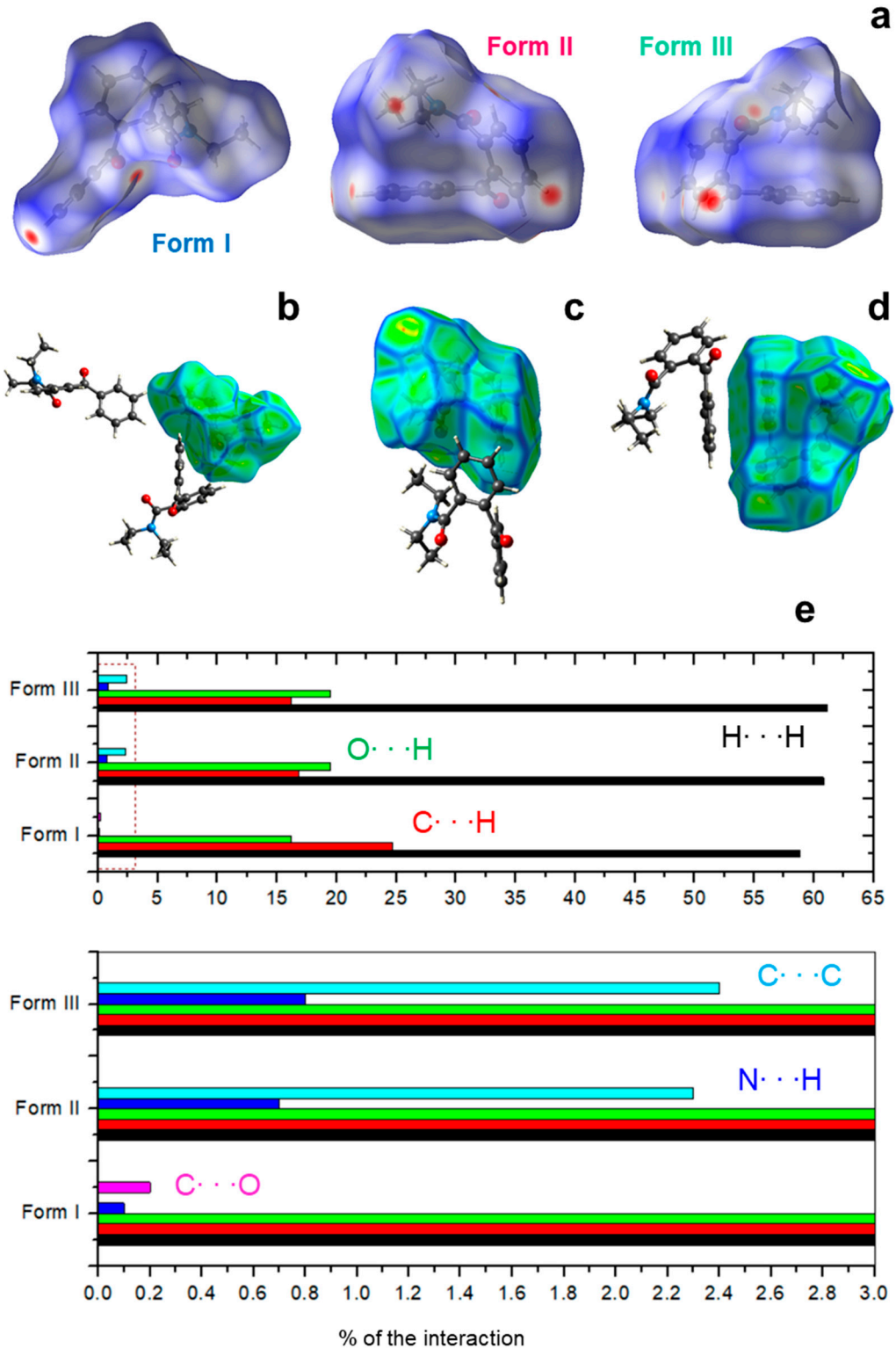

Figure 4. Hirshfeld surfaces for the three known forms of BDB (**a**), herringbone stacking present in form I (**b**) and forms II and III (**c**), cofacial π–π interaction present in forms II and III (**d**) and distribution of the intermolecular interactions for all forms of BDB with the area below 3.0% zoomed-in (**e**).

Fingerprint plots detail the composition of the intermolecular interactions for these crystal structures and are observed for forms I–III in Figures S5–S7. Figure 4e illustrates the contribution of the interactions to the Hirshfeld Surfaces. The majority of the interactions

occur between hydrogens atoms for all three forms (H···H). Hydrogen bonds between carbon-hydrogen, oxygen-hydrogen and nitrogen-hydrogen are also present in all forms. The variation of the molecular conformation for these polymorphs directly affects the composition of these interactions. Form I have a lower percentage of H···H (58.8%), O···H (16.2%) and N···H (0.1%) than forms II and III. In comparison with form II, these values slightly increase to 60.8% (H···H), 19.5% (O···H) and 0.7% (N···H). The larger difference in the composition is related to C···H interactions, which occupy a quarter of the interactions for form I (24.7%) while are only present in 16.8% of form II's HS interactions. In these molecules there is also the presence of π–π interactions between carbon-carbon (form II, 2.3%; form III, 2.4%), as can be observed by the zoomed-in graph in Figure 4e.

Since there are no significant differences in relation to the bonds, angles and dihedral angles for forms II and III of BDB, the packing of these molecules was compared using the crystal packing similarity tool within the Mercury software [32,33]. The program was set to cluster sizes of twenty molecules with a 20% tolerance of distance and angle and using form II as the reference structure (Figure 5, molecules in grey). Only fifteen out of the total twenty molecules of form III packed with the reference structure (molecules in green), while the remaining five molecules (in red) have a displacement of 3.3 Å in relation to the reference molecules. Thus, the differences between these two polymorphs are related only to the long-range packing of molecules in the crystal structure.

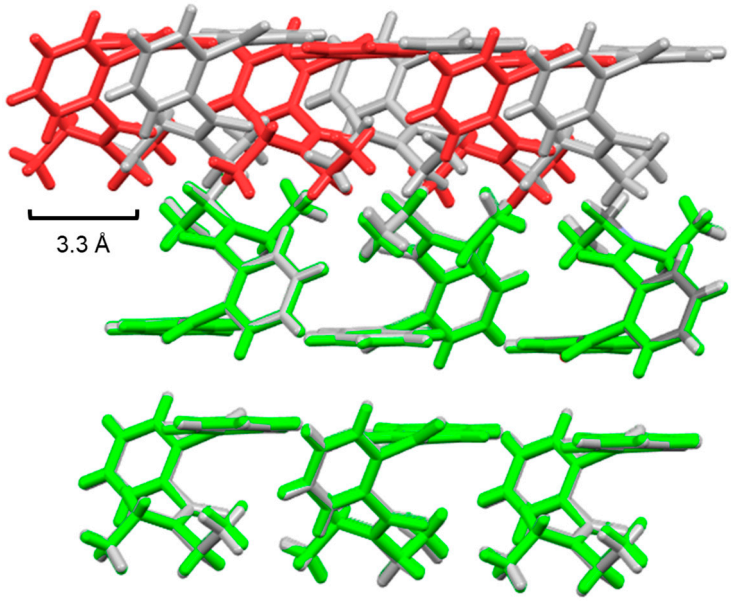

Figure 5. Crystal packing similarity between forms II (in grey—reference) and III (colored). Green are molecules that confirm similar packing of forms II and III for 15 out of 20 molecules. Molecules in red do not match with the packing of form II.

3.5. Thermal Characterization

The thermal stability of BDB was analyzed using thermogravimetric analysis (TGA) and differential scanning calorimetry (DSC). TGA analysis of form II showed that the sample starts degrading above 200 °C, and the mass is lost completely below 320.0 °C, as illustrated in Figure S8 and Table S3.

Differential scanning calorimetry (DSC) of the isolated form II shows no phase transition within the temperature range between −50 and 90 °C (Figure S9, Table S3). The experiment was performed in two heating-cooling cycles with the same temperature range. In the first heating cycle, it is possible to observe a large endothermic peak with an onset temperature of 51.2 °C, consistent with the fusion temperature of the sample, melting enthalpy of 24.3 kJ/mol and melting entropy of 75.0 J/K·mol (9.0 R, where R = 8.314 J/K·mol—gas constant). This result is similar to the melting point of the sample first synthesized by

Projotiva et al. (51.5 °C). Thus, identified here is the form synthesized by Projotiva et al. as form II [13]. In the second heating cycle, most of form II is amorphous, and it is possible to observe the glass transition temperature at −20.8 °C and a small endothermic peak with an onset of 53.9 °C, still consistent with the melting of form II. In the second heating, the melting enthalpy observed was 0.6 kJ/mol and melting entropy of 1.7 J/K·mol (0.2R). In both cooling cycles, the sample presents low intensity cracking peaks at −42.8 °C ($\Delta H_{crack,1}$ = −0.05 kJ/mol) and −42.9 °C ($\Delta H_{crack,2}$ = −0.01 kJ/mol), respectively, which does not have an influence on the formation of a new polymorph of BDB.

3.6. Thermal Stability of Form II

X-ray powder diffraction in different temperature points was used to confirm the stability of form II and would not convert into another form when submitted to heating or cooling. The first variable temperature experiment was performed heating the sample from room temperature up to the melting point of form II (51.2 °C). Details of this experiment can be obtained in the Supporting Information, Figure S10 and Table S4.

As observed with the DSC experiment, no solid-solid phase transition occurred between room temperature and the melting of form II. Figure 6 reveals that the sample is stable in different temperature points, and the compression of the unit cell is neglectable: Less than 0.5% for *a*, *b*, *c* and β and less than 1.0% in volume. The average unit cell for this experiment is *a* = 13.71(2), *b* = 8.38(2), *c* = 26.83(3) Å and β = 90.52(7)°. There was no variation in the crystal system or space group (monoclinic, I2/a) during the heating, and the compound was completely molten at 60 °C. Once the system cooled back to room temperature, the compound recrystallized over the glass slide as form II with preferred orientation in the *c* direction (Figure S11).

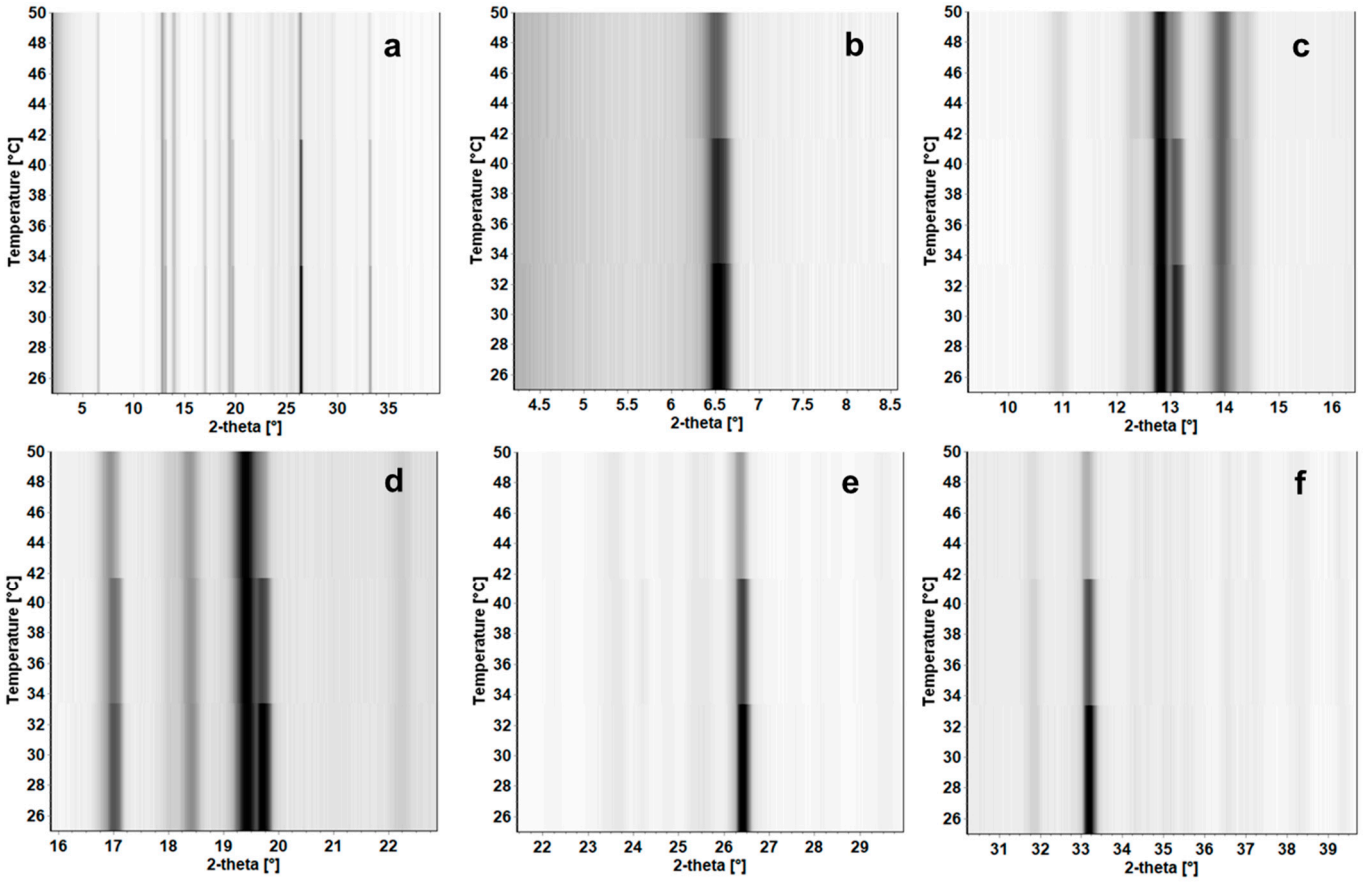

Figure 6. Isolines representing the compression of the unit cell at high temperature for form II for 2θ range between 2 and 40° (**a**) and zoomed-in 2θ regions between 4.0 and 8.5° (**b**), 9.5 and 6.5° (**c**), 16 and 22.5° (**d**), 22.0 and 29.5° (**e**) and 30.5 and 39.5° (**f**).

3.7. Temperature Induced Polymorphism of BDB

In the second experiment performed with form II, the sample was cooled to −170 °C and heated to 55 °C (3.8 °C higher than the melting point of form II). Details of this experiment can be obtained in the Supporting Information, Figure S12 and Table S5. From room temperature down to −170 °C, form II was stable and did not convert into any different form. However, the sample showed a transition into a new form in temperatures over −93 °C. The phase transition between these forms is subtle (Figure 7a) but easy to observe when analyzing the isolines for the variable temperature experiment peak by peak, where peaks located around 18.5, 23.7 and 29.5° from the monoclinic form II merge into a single peak (Figure 7b,c,f), single peaks become bifurcated (around 25.5°, Figure 7d) or peaks are shifted (from 26.7 to 26.2°, Figure 7e), indicating a phase transition occurring in the temperature range between −93 and −73 °C.

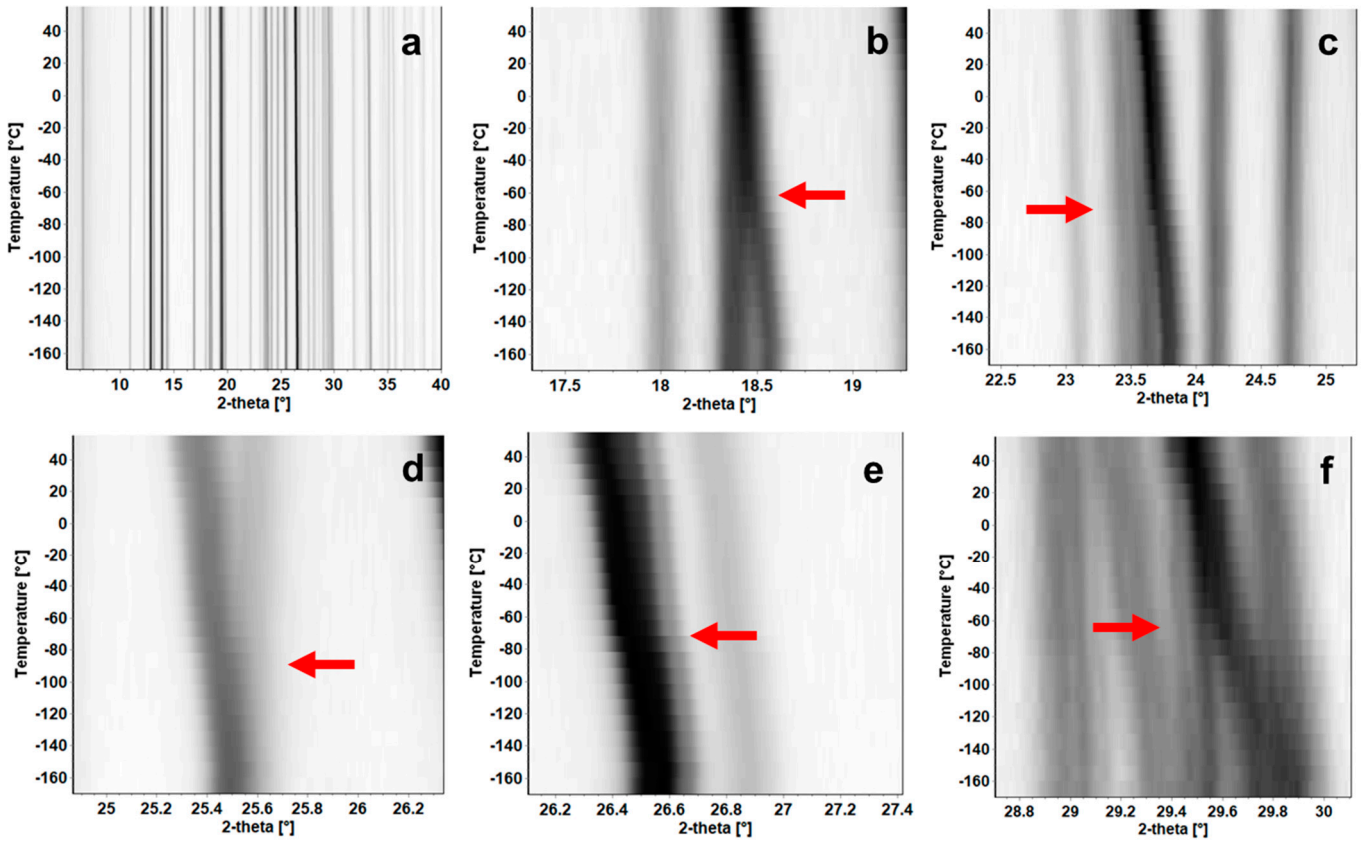

Figure 7. Isolines representing the phase transformation of form II into form IV for 2θ range between 5 and 40° (**a**) and zoomed-in 2θ regions between 17.0 and 20.0° (**b**), 22.5 and 25.5° (**c**), 24.5 and 26.5° (**d**), 26.0 and 27.5° (**e**) and 26.5 and 30.2° (**f**).

The powder diffraction patterns were indexed to obtain the unit cell parameters for each different point, and Figure 8 shows the variation of the unit cell parameters according to the temperature. Once cooled, form II is stable between −170 and −113 °C. These values oscillate around the average value for this temperature range of a = 13.696(6), b = 8.440(3), c = 26.796(16) Å with no variation in the crystal system or space group (monoclinic, I2/a). Figure 8a and Table S5 exhibit the lattice values a, b and c. Figure 8b shows the angle β decreasing almost linearly towards 90° when increasing the temperature, but below −113 °C. The average value of β before the phase transition is 90.485(25)°. These average values are within 1.0% difference of the lattice parameters obtained by single-crystal X-ray diffraction for form II.

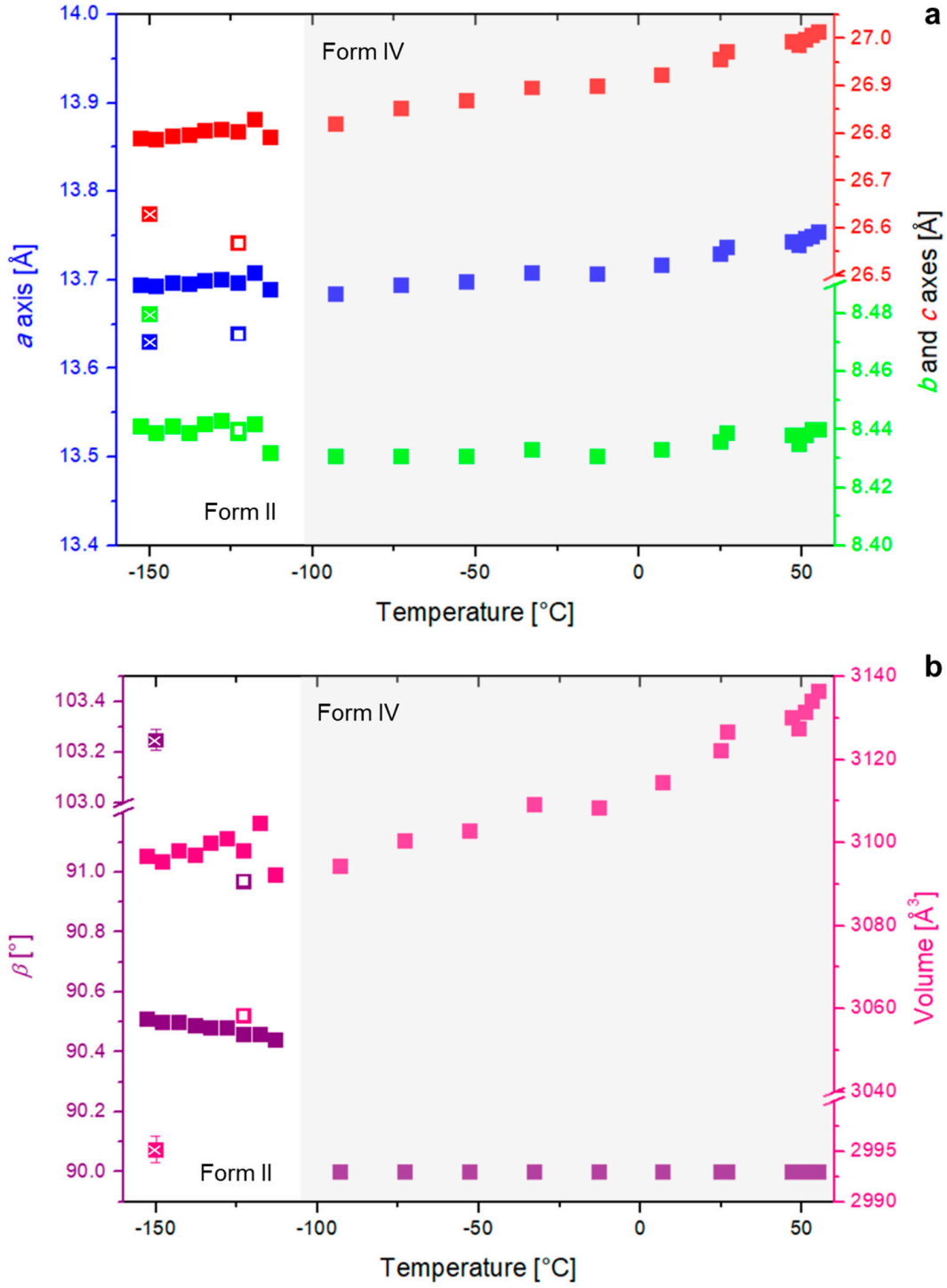

Figure 8. Variation of form II of BDB in different temperature points of the lattice parameters (**a**) and of β angle and volume (**b**). Forms II and III are represented by the white squares and crosses, respectively. Form I was omitted from the graphs. Some standard deviations are too small to be observed in the graphs.

For temperatures higher than −53 °C, a new phase, denoted as form IV, is observed. This solid–solid phase transition was not observed via DSC as the instrument used could only reach −50 °C, and the phase transition starts at lower temperatures. This indicates that once cooled, increasing the temperature induces the transition to an orthorhombic form.

When indexed, the new orthorhombic form had unit cell parameters at 25 °C as: a = 13.730(2), b = 8.4361(10) and c = 26.955(3) Å (R_p = 10.26%, R_{wp} = 12.98%), and space group *I*mmm. In comparison with form II, there was an insignificant decrease of lengths a,

b and *c* during the phase transition temperature range (−93 to −73 °C) of 0.17% for *a*, 0.13% for *b* and 0.03% for the *c*-axis, and a decrease of 0.33% in volume. The greatest temperature response was made by the change from the monoclinic to orthorhombic crystal system, and consequently, β angle decreasing 0.51%. The small changes in the dimensions when the phase transition occurs indicate that there are no significant variations in the molecular arrangement of BDB.

Once the phase transformation between forms II and IV occurs, form IV is stable through higher temperatures up to 55 °C. The unit cell for this form has a higher response to temperature, where it expands when heated: *a* increases 0.51%, *b* increases 0.11% and *c* increases 0.73%, with an overall expansion of the unit cell equals 1.35% of the volume. Details of the indexed results for each temperature point can be obtained in the Supporting Information, Table S5.

4. Conclusions

A polymorphic profile was identified for 2-benzoyl-*N*,*N*-diethylbenzamide (BDB) at room temperature, where two new forms of the compound were obtained: forms II and III. The crystal structure of these forms was obtained, and a structural comparison shows similar molecular conformation between the two forms, differing only in the long-range molecular packing. In comparison with the known form of BDB (form I [15]), great differences in the molecular conformation and packing arrangements between these forms were observed.

The new form II was identified as the same form obtained in the literature with a melting point of 51.2 °C [13], and this form is stable at room temperature and when it was heated. There is another form of BDB, with a melting point range between 76 and 77 °C [14,19], which is still not identified. Unfortunately, this work was not able to isolate forms I and III in the recrystallization trials; thus the melting profile of these forms was not obtained. However, due to the specific conditions form III was recrystallized, form I is a possible candidate for the melting point range of 76–77 °C.

When submitted to low temperatures (−170 °C), a phase transformation of form II was induced when re-heating the sample. In this case, form II transitions from the monoclinic into the orthorhombic crystal system. This new phase, form IV, is also body-centered and insignificantly different in the unit cell parameters when compared to form II, indicating that although the phase transition occurred, the molecular arrangements for form IV are similar to form II. Form IV has a higher melting point than form II (>55.0 °C); however, the crystal structure and melting profile of this form must still be obtained.

Supplementary Materials: The following are available online at https://www.mdpi.com/article/10.3390/cryst11081004/s1, Scheme S1: Synthesis route of 2-benzoyl-*N*,*N*-diethylbenzamide (BDB); Figure S1: ^{1}H NMR spectra of 2-benzoyl-*N*,*N*-diethylbenzamide in $CDCl_3$ solution; Table S1: Label and torsion angle values used in the database survey for the nine structures analyzed; Figure S2: ^{13}C NMR spectra of 2-benzoyl-*N*,*N*-diethylbenzamide in $CDCl_3$ solution; Table S2: Calculated values of volume, area, globularity and asphericity for the Hirshfeld surfaces and voids of the three forms of 2-benzoyl-*N*,*N*-diethylbenzamide; Figure S3: Powder diffraction patterns for the calculated form I (in black. CSD refcode = BERDOS), calculated form II (in red), calculated form III (in blue), synthesis product batch (in cyan), BDB recrystallized by hexane:chloroform (in pink) and recrystallized by dichloromethane (in beige); Table S3: TGA and DSC parameters and results for the sample BDB; Figure S4: Molecular structure of the compounds mentioned in the database survey; Table S4: Variation of the unit cell parameters according to the temperature for the sample BDB; Figure S5: Hirshfeld surfaces and fingerprint plots showing all interactions (a), only C···H/H···C interactions (b), only O···H/H···O interactions (c), only N···H/H···N interactions (d), only H···H interactions (e), only C···O/O···C interactions (f) and voids in the unit cell (g) of the sample form I (refcode: BERDOS); Table S5: Variation of the unit cell parameters according to the temperature for the sample BDB; Figure S6: Hirshfeld surfaces and fingerprint plots showing all interactions (a), only C···H/H···C interactions (b), only O···H/H···O interactions (c), only N···H/H···N interactions (d), only H···H interactions (e), only C···C interactions (f) and voids in the unit cell (g) for the sample form II;

Figure S7: Hirshfeld surfaces and fingerprint plots showing all interactions (a), only C···H/H···C interactions (b), only O···H/H···O interactions (c), only N···H/H···N interactions (d), only H···H interactions (e), only C···C interactions (f) and voids in the unit cell (g) for the sample form III; Figure S8: TGA curve heating the sample form II from 30 to 500 °C with a step of 10 °C/min; Figure S9: DSC heating and cooling curves for the sample form II. The curve in green represents the 1st heating (0.50 °C/min), in blue the 1st cooling (0.75 °C/min), in purple the 2nd heating and in brown the 2nd cooling; Figure S10: Diffractograms for variable temperature X-ray powder diffraction experiments at five different temperature points (T range between 25 and 60 °C); Figure S11: Diffractograms at room temperature after the crystallization from the melt; Figure S12: Diffractograms for variable temperature X-ray powder diffraction experiments at 24 different temperature points (*T* range between −170 and 55 °C).

Author Contributions: Conceptualization, L.S.d.M. and Y.H.G.; methodology, L.S.d.M.; synthesis, E.G.; recrystallization, L.S.d.M. and R.O.; XRPD and VT-XRPD, L.S.d.M. and J.L.; SXD, A.R.K.; formal analysis, L.S.d.M.; writing—original draft preparation, L.S.d.M.; writing—review and editing, all authors; supervision, Y.H.G.; project administration, Y.H.G.; funding acquisition, Y.H.G. All authors have read and agreed to the published version of the manuscript.

Funding: This research was funded by the Belgian National Fund for Scientific Research (FNRS) for financial support through research projects Phasetrans n° T.0058.14 and 2D to 3D No. 30489208. Financial support from ULB and the French Community of Belgian (ARC SADI) is also gratefully acknowledged.

Data Availability Statement: The raw data presented in this study are available on request from the corresponding authors. All published crystal structures used in this work are referenced in the main text and can be obtained from CCDC. Crystal structures of forms II and III of BDB have been deposited at CCDC with deposition numbers 2102737 and 2102738. These data can be obtained free of charge via email at deposit@ccdc.cam.ac.uk, from the website http://www.ccdc.cam.ac.uk/conts/retrieving.html (accessed on 10 August 2021) or CCDC, 12 Union Road, Cambridge CB2 1EZ, UK; Fax: +44 1223 336033. XRPD, DSC, TGA, NMR and synthesis descriptions are given in the Supporting Information.

Acknowledgments: The authors thank the National Crystallographic Service at the University of Southampton for collecting the data to obtain the crystal structure of form II of BDB. We would also like to thank CNPq (Conselho Nacional de Desenvolvimento Científico e Tecnológico) and the Science without borders program (SwB/CsF) for the flexibility to perform this research. We gratefully acknowledge financial support from Action de Recherche Concertée—ULB under Project SADI (n° 20061), and the Fonds de la Recherche Scientifique (FNRS) and the Fonds voor Wetenschappelijk Onderzoek—Vlanderen (FWO) under EOS project (n° 30489208). R.O. has benefited from IF@ULB fellowship under the COFUND MSCA program.

Conflicts of Interest: The authors declare no conflict of interest.

References

1. Olovsson, I.; Jönsson, P.-G. *The Hydrogen Bond. Recent Developments in Theory and Experiments*; North-Holland: Amsterdam, The Netherlands, 1976.
2. Caira, M.R. Crystalline Polymorphism of Organic Compounds. In *Design of Organic Solids*; Weber, E., Aoyama, Y., Caira, M.R., Desiraju, G.R., Glusker, J.P., Hamilton, A.D., Melendez, R.E., Nangia, A., Eds.; Springer: Berlin/Heidelberg, Germany, 1998; pp. 163–208.
3. Bernstein, J. *Polymorphism in Molecular Crystals*; Oxford University Press: Oxford, UK, 2007; ISBN 9780199236565.
4. Brog, J.-P.; Chanez, C.-L.; Crochet, A.; Fromm, K.M. Polymorphism, what it is and how to identify it: A systematic review. *RSC Adv.* **2013**, *3*, 16905–16931. [CrossRef]
5. Sarma, B.; Chen, J.; Hsi, H.-Y.; Myerson, A.S. Solid forms of pharmaceuticals: Polymorphs, salts and cocrystals. *Korean J. Chem. Eng.* **2011**, *28*, 315–322. [CrossRef]
6. Lipinski, C.A. Drug-like properties and the causes of poor solubility and poor permeability. *J. Pharmacol. Toxicol. Methods* **2000**, *44*, 235–249. [CrossRef]
7. Niazi, S.K. The scope of preformulation studies. In *Handbook of Preformulation Chemical, Biological, and Botanical Drugs*; Informa Healthcare: New York, NY, USA, 2007; pp. 57–86.
8. Lee, R.; Yufit, D.S.; Probert, M.R.; Steed, J.W. High Pressure/Low Temperature Polymorphism in 2,6-Dimethylpyridine–Formic Acid Cocrystals. *Cryst. Growth Des.* **2017**, *17*, 1647–1653. [CrossRef]

9. Cacela, C.; Baudot, A.; Duarte, M.; Matos-Beja, A.; Silva, M.R.; Paixão, J.A.; Fausto, R. Low temperature polymorphism in 3-amino-1-propanol. *J. Mol. Struct.* **2003**, *649*, 143–153. [CrossRef]
10. Maria, T.M.R.; Castro, R.A.E.; Silva, M.R.; Ramos, M.L.; Justino, L.; Burrows, H.D.; Canotilho, J.; Eusébio, M.E.S. Polymorphism and melt crystallisation of racemic betaxolol, a β-adrenergic antagonist drug. *J. Therm. Anal. Calorim.* **2013**, *111*, 2171–2178. [CrossRef]
11. Delaney, S.P.; Smith, T.M.; Pan, D.; Yin, S.X.; Korter, T.M. Low-Temperature Phase Transition in Crystalline Aripiprazole Leads to an Eighth Polymorph. *Cryst. Growth Des.* **2014**, *14*, 5004–5010. [CrossRef]
12. Foces-Foces, C.; Roux, M.V.; Notario, R.; Segura, M. Thermal behavior and polymorphism in medium–high temperature range of the sulfur containing amino acids l-cysteine and l-cystine. *J. Therm. Anal. Calorim.* **2011**, *105*, 747–756. [CrossRef]
13. Protiva, M.; Vejdělek, Z.J. Synthetic antispasmodics. I. Some new basic esters. *Collect. Czechoslov. Chem. Commun.* **1950**, *15*, 541–551. [CrossRef]
14. Lynn, J.W.; English, J. Reaction of *N,N*-Dialkylbenzamides with Sodium. *J. Org. Chem.* **1951**, *16*, 1546–1555. [CrossRef]
15. Sakamoto, M.; Kobaru, S.; Mino, T.; Fujita, T. Absolute asymmetric synthesis by nucleophilic carbonyl addition using chiral crystals of achiral amides. *Chem. Commun.* **2004**, *4*, 1002–1003. [CrossRef] [PubMed]
16. Jing, K.; Yao, J.P.; Li, Z.Y.; Li, Q.L.; Lin, H.S.; Wang, G.W. Palladium-Catalyzed Decarboxylative *ortho* -Acylation of Benzamides with α-Oxocarboxylic Acids. *J. Org. Chem.* **2017**, *82*, 12715–12725. [CrossRef] [PubMed]
17. Laha, J.K.; Patel, K.V.; Sharma, S. Palladium-Catalyzed Decarboxylative Ortho-Acylation of Tertiary Benzamides with Arylglyoxylic Acids. *ACS Omega* **2017**, *2*, 3806–3815. [CrossRef] [PubMed]
18. Park, J.; Park, E.; Kim, A.; Lee, Y.; Chi, K.W.; Kwak, J.H.; Jung, Y.H.; Kim, I.S. Rhodium-Catalyzed Oxidative *ortho*-Acylation of Benzamides with Aldehydes: Direct Functionalization of the sp ^{2} C–H Bond. *Org. Lett.* **2011**, *13*, 4390–4393. [CrossRef] [PubMed]
19. Seganish, W.M.; DeShong, P. Application of Directed Orthometalation toward the Synthesis of Aryl Siloxanes. *J. Org. Chem.* **2004**, *69*, 6790–6795. [CrossRef] [PubMed]
20. Wei, W.-T.; Liu, Y.; Ye, L.-M.; Lei, R.-H.; Zhang, X.-J.; Yan, M. Rapid synthesis of isoquinolinones by intramolecular coupling of amides and ketones. *Org. Biomol. Chem.* **2015**, *13*, 817–824. [CrossRef]
21. Hursthouse, M.B.; Coles, S.J. The UK National Crystallography Service; its origins, methods and science. *Crystallogr. Rev.* **2014**, *20*, 117–154. [CrossRef]
22. Rigaku Oxford Diffraction. *CrysAlisPRO Software System*; Version 1.171.40.82a; Rigaku Corporation: Oxford, UK, 2020.
23. Sheldrick, G.M. A short history of *SHELX*. *Acta Crystallogr. Sect. A Found. Crystallogr.* **2008**, *64*, 112–122. [CrossRef]
24. Palatinus, L.; Chapuis, G. *SUPERFLIP*—A computer program for the solution of crystal structures by charge flipping in arbitrary dimensions. *J. Appl. Crystallogr.* **2007**, *40*, 786–790. [CrossRef]
25. Sheldrick, G.M. Crystal structure refinement with *SHELXL*. *Acta Crystallogr. Sect. C Struct. Chem.* **2015**, *71*, 3–8. [CrossRef]
26. Farrugia, L.J. *ORTEP* -3 for Windows—A version of *ORTEP* -III with a Graphical User Interface (GUI). *J. Appl. Crystallogr.* **1997**, *30*, 565. [CrossRef]
27. Cottrell, S.J.; Olsson, T.S.G.; Taylor, R.; Cole, J.C.; Liebeschuetz, J.W. Validating and Understanding Ring Conformations Using Small Molecule Crystallographic Data. *J. Chem. Inf. Modeling* **2012**, *52*, 956–962. [CrossRef]
28. Bruno, I.; Cole, J.; Kessler, M.; Luo, J.; Motherwell, W.D.S.; Purkis, L.H.; Smith, A.B.R.; Taylor, R.; Cooper, R.I.; And, S.E.H.; et al. Retrieval of Crystallographically-Derived Molecular Geometry Information. *J. Chem. Inf. Comput. Sci.* **2004**, *44*, 2133–2144. [CrossRef] [PubMed]
29. Albinati, A.; Willis, B.T.M. The Rietveld method in neutron and X-ray powder diffraction. *J. Appl. Crystallogr.* **1982**, *15*, 361–374. [CrossRef]
30. Rietveld, H.M. A profile refinement method for nuclear and magnetic structures. *J. Appl. Crystallogr.* **1969**, *2*, 65–71. [CrossRef]
31. Altomare, A.; Cuocci, C.; Giacovazzo, C.; Moliterni, A.; Rizzi, R.; Corriero, N.; Falcicchio, A. *EXPO2013*: A kit of tools for phasing crystal structures from powder data. *J. Appl. Crystallogr.* **2013**, *46*, 1231–1235. [CrossRef]
32. Macrae, C.F.; Edgington, P.R.; McCabe, P.; Pidcock, E.; Shields, G.; Taylor, R.; Towler, M.; van de Streek, J. *Mercury*: Visualization and analysis of crystal structures. *J. Appl. Crystallogr.* **2006**, *39*, 453–457. [CrossRef]
33. Macrae, C.F.; Bruno, I.J.; Chisholm, J.A.; Edgington, P.R.; McCabe, P.; Pidcock, E.; Rodriguez-Monge, L.; Taylor, R.; Streek, J.V.D.; Wood, P.A. *Mercury CSD 2.0*—New features for the visualization and investigation of crystal structures. *J. Appl. Crystallogr.* **2008**, *41*, 466–470. [CrossRef]
34. Le Bail, A.; Duroy, H.; Fourquet, J.L. Ab-initio structure determination of LiSbWO6 by X-ray powder diffraction. *Mater. Res. Bull.* **1988**, *23*, 447–452. [CrossRef]
35. Spackman, M.A.; Jayatilaka, D. Hirshfeld surface analysis. *CrystEngComm* **2009**, *11*, 19–32. [CrossRef]
36. Spackman, M.A.; McKinnon, J.J. Fingerprinting intermolecular interactions in molecular crystals. *CrystEngComm* **2002**, *4*, 378–392. [CrossRef]
37. Spackman, P.R.; Turner, M.J.; McKinnon, J.J.; Wolff, S.K.; Grimwood, D.J.; Jayatilaka, D.; Spackman, M.A.J. CrystalExplorer: A program for Hirshfeld surface analysis, visualization and quantitative analysis of molecular crystals. *Appl. Cryst.* **2021**, *54*, 1006–1011. [CrossRef] [PubMed]
38. Turner, M.J.; McKinnon, J.J.; Jayatilaka, D.; Spackman, M.A. Visualisation and characterisation of voids in crystalline materials. *CrystEngComm* **2011**, *13*, 1804–1813. [CrossRef]

39. Sakamoto, M.; Sekine, N.; Miyoshi, H.; Mino, T.; Fujita, T. Absolute Asymmetric Phthalide Synthesis via the Solid-State Photoreaction of *N,N*- Disubstituted 2-Benzoylbenzamides Involving a Radical Pair Intermediate. *J. Am. Chem. Soc.* **2000**, *122*, 10210–10211. [CrossRef]
40. Valente, E.J.; Martin, S.B.; Sullivan, L.D. Pseudoacids. II. 2-Acylbenzoic Acid Derivatives. *Acta Crystallogr. Sect. B Struct. Sci.* **1998**, *54*, 264–276. [CrossRef]
41. Guo, S.; Sun, L.; Liu, Y.; Ma, N.; Zhang, X.; Fan, X. Rh(III)-Catalyzed Oxidative Spirocyclization of Isoquinolones with α-Diazo-1,3-indandiones. *Org. Lett.* **2019**, *21*, 4082–4086. [CrossRef] [PubMed]